ESTIMATIONS OF ABL FLUXES AND OTHER TURBULENCE PARAMETERS FROM DOPPLER LIDAR DATA

by

Tzvi Gal-Chen and Mei Xu

University of Oklahoma School of Meteorology
Norman OK 73019

and

Wynn Eberhard

National Oceanic and Atmospheric Administration

Wave Propagation Laboratory
Boulder CO 80303

ABSTRACT

Techniques for extractions boundary layer parameters from measurements of a short-pulse ($\approx$ 1 μs) CO_2 Doppler Lidar (λ = 10.6 μm) are described. The Lidar is operated by the National Oceanic and Atmospheric Administration (NOAA) Wave Propagation Laboratory (WPL). The measurements are those collected during the First International Satellites Land surface Climatology Project (ISLSCP) Field Experiment (FIFE). The radial velocity measurements have a range resolution of 150 m. With a pulse repetition rate of 20 Hz, it is possible to perform scannings in two perpendicular vertical planes (x-z and y-z) in $\approx$ 72 s. By continuously operating the Lidar for about an hour, one can extract stable statistics of the radial velocities. Assuming that the turbulence is horizontally homogeneous, we have estimated the mean wind, its standard deviations, and the momentum fluxes. From the vertically pointing beam we have estimated the first, second, and, third moments of the vertical velocity. Spectral analysis of the radial velocities is also performed from which, by examining the amplitude of the power spectrum at the inertial range, we have deduced the kinetic energy dissipation. Finally, using the statistical form of the Navier-Stokes equations, the surface heat flux is derived as the residual balance between the vertical gradient of the third moment of the vertical velocity and the kinetic energy dissipation. With the exception of the vertically pointing beam, an individual radial velocity estimate is accurate only to ± 0.7 ms^{-1}. Combining many measurements would normally reduce the error provided that, it is un-biased and un-correlated. The nature of some of the algorithms however, is such that, biased and correlated errors may be generated even though the "raw" measurements are not. We have developed data processing procedures that eliminate bias and minimize error correlation. Once bias and error correlations are accounted for, the large sample size is shown to

reduce the errors substantially. We show for instance that, a single momentum flux estimate has an accuracy of ± 2 m^2s^{-2} but, when combined with other measurements the error can be reduced to ± 0.10 m^2s^{-2}. The principal features of the derived turbulence statistics for two case studies (11 July 1987 16:11-17:10 UTC and 17:29-18:10 UTC) are as follows:

(a) The mean surface wind is from the south and has a speed of $\approx$ 15 ms^{-1}. There is a southerly jet at 1 km above the surface. The wind in the direction normal to the surface wind is becoming more westerly with height.

(b) The derived momentum fluxes in the mixed layer agree with the unfiltered airplane measurements. They are of the order of $\approx$ 0.5 m^2s^{-2} near the surface and are retarding the southerly wind. At the stable layer, the momentum fluxes are counter-gradient; they remain negative even though the southerlies are diminishing with height; and furthermore they are concentrated in thin layers. By spectrally analysing the vertical beam, we have identified the Brunt Väisälä frequency as the dominant frequency in the stable layer. The available evidence suggests that the large counter-gradient fluxes are due to a critical layer singularity. Under these conditions gravity waves flux divergence may be large. Current General Circulations Models (GCM's) generally do not parameterize counter-gradient momentum transport. If the phenomenon is prevalent, our study suggests that inclusion of such an effect may be important.

(c) The spectrum of the wind near the surface has a $-5/3$ power law at the inertial range. The heat flux estimate is 100 ± 20 Wm^{-2} in apparent agreement with the surface stations estimate but, systematically larger than the filtered airplane data.

1. Introduction and Goals

The purpose of this paper is two fold. First we wish to describe in some detail an analysis technique of a single Doppler Lidar (for Light Detection and Range) data which allows the estimation of the following turbulence parameters: a) mean wind $(\bar{u}, \bar{v}, \bar{w})$ where $\overline{(\ )}$ is a symbol for some kind of average (to be defined in section 4) and (u, v, w) are the Cartesian velocities in the (x, y, z) directions respectively; b) the variance $(\overline{u'^2}, \overline{v'^2}, \overline{w'^2})$, where $(\ )'$ is a symbol for the deviations from the mean; c) the part of the covariance associated with the vertical fluxes of horizontal momentum $(\overline{u'w'}, \overline{v'w'})$ and d) the third moment of the vertical velocity, $\overline{w'^3}$, the kinetic energy dissipation ϵ and the surface heat flux.

A second objective of our research is to study the behaviour of the convective Planetary Boundary Layer (PBL) and it's overlying stable region under the condition of strong surface wind, moderate surface heat flux and a low level jet. We shall sometimes refer to the PBL as ABL (Atmospheric Boundary Layer).

The scale of motions investigated in our study are in the range of 150 m - 12 km, too small to be resolved by current and near future General Circulation Models (GCM's); yet generally recognised to have an important influence on the larger scales. The proper "parameterisations" of these processes remains an important unsolved issue despite several decades of research (Wyngaard, 1983). One reason for the apparent slow progress is the requirements for acquiring large samples in a relatively short time so that, on the one hand the statistics are stable but, on the other hand the sampling time must be sufficiently short, so that evolution can be ignored (Wyngaard, 1983). As a result "too many models are chasing too little data...". Due to an ability to measure simultaneously a ray of points (actually resolution volumes) remote sensing by Doppler Lidars and Radars could contribute significantly to alleviate the sampling problems . In

our case for instance, a ray (containing fifty to a hundred data points) could be sensed in 1/20 s. Such sampling rate is an order of magnitude faster than in situ observations (e.g by aircraft or meteorological towers).

Another unresolved issue in atmospheric turbulence is the similarities and differences between stratified and convective turbulence (Lilly, 1982) as well as the interaction between the convection in the mixed layer and the waves in the stable region above (Kuetner et al., 1987). The Lidar data that we have collected include observations in both the mixed layer and parts of the overlying stable region. Thus, it is possible to compare theories with observations.

The data base for this study are measurements taken during the First International Satellites Land Surface Climatology Project (ISLSCP) Field Experiment (FIFE) in Manhattan, KS. Since, the experimental technique, the data reduction and the hardware are still under development (Eberhard et al., 1989) we confine ourselves here to two case studies (11 July 1987, 16:11-17:10 UTC and 17:29-18:20 UTC). The Central Standard Time (CST) is lagging five hours behind the Coordinated Universal Time (UTC).

2. System Characteristics

For the purpose of this presentation we assume that the Doppler Lidar is simply a "black box" which measures the frequency shift between a transmitted (coherent) pulse and the backscattered power. The frequency difference is a measure of the velocity component toward or away from the Lidar (i.e., the radial velocity). The frequency ω of the transmitted pulse is given by $\omega = c2\pi/\lambda$ where λ is the wave length of the emitted radiation (10.6 μm) and c the speed of light. The pulse duration ΔT is $1\mu s$ which means that at any given time the recorded backscattered power is actually a superposition of returns from several ranges re-

flecting different parts of the pulse. The range resolution ΔR (i.e., the length of the line interval which corresponds to backscattered power recorded at the same time) is then given by $2\Delta R = c\Delta T$. This means in our case that $\Delta R = 150\,\mathrm{m}$. The factor 2 takes into account that the pulse goes out and is reflected back.

The minimum range below which velocity estimates are not reliable is 600 m. The maximum range above which the signal/noise ratio is too low to permit radial wind estimates depends mostly on aerosols content and absolute humidity (Eberhard et al., 1989). For these particular case studies it appears to be 6 km in the horizontal and 2 km in the vertical. Since the Lidar scanner can move vertically and horizontally, one can combine "forward" and "backward" shots to obtain at the surface velocity measurements along a 12 km line with a "gap" of seven range gates in the centre. As one moves upward the lines becomes progressively shorter since no useful returns are available above 2 km. Finally it should be mentioned that the pulse repetition rate is 20 Hz (i.e., 20 pulses are being fired in one second). With the exception of the vertical direction, three pulses are combined to get a more stable (less noisy) velocity estimate (± 0.70 ms^{-1}). In the vertical direction we use twelve shots to get a more accurate estimate (± 0.35 ms^{-1}) of the vertical velocity .

Combining the above information it is concluded that, a radial can be sensed in 0.15 s. Since a single horizontal beam contains 37 useful velocity measurements the over all sampling rate is several orders of magnitude faster than typical sampling rate of an airplane. Further details of the Lidar characteristics may be found in Eberhard et al. (1989).

3. Experimental Design

The experimental design is a compromise between two conflicting require-

ments. First one a wishes to cover every resolution volume in the boundary layer (i.e., to observe a contiguous sequence of volumes, each approximately $150\,m^3$ in size. Second, it is deemed desirable to scan the entire boundary layer fast enough so that, the assumption of a statistical steady state would be valid. Unfortunately, taking into account the system characteristics it is not possible to satisfy the above requirements simultaneously. Instead of covering the entire volume we have decided to scan in two mutually orthogonal planes. For horizontally homogeneous turbulence the choice of the two orthogonal planes could be arbitrary; knowledge of the statistics in one coordinate system implies knowledge in any other coordinate system (Batchelor, 1956). For convenience however, one plane say (x-z) is formed by the vertical and the line in the direction of the mean surface wind. The other plane (y-z) is the vertical and the direction orthogonal to the mean surface wind. This type of scanning precluded an estimation of $\overline{u'v'}$. To accomplish the scanning described above an a'priori knowledge of the mean surface wind need to be assumed and this can be obtained from a single Velocity Azimuth Display (VAD) scanning (Kropfli, 1986).

The actual implementation of the scan (called also RHI for Range Height Indicator) consists of first positioning the Lidar (at zero elevation) in the direction of the mean surface wind. Keeping the horizontal direction fixed, increments in elevation Θ are made until an elevation Θ_1 is achieved. Both Θ_1 and $\Delta\Theta$ (the increment) are controllable. In our case we have taken $\Delta\Theta \approx 1°$ and $\Theta_1 = 42°$. From the position Θ_1 one can move the Lidar as quickly as possible to a vertical scanning, which is $\pm 2°$ away from the zenith .This is followed by a quick descent to Θ_1 . From Θ_1 the Lidar moves down to zero elevation by decrements of $\Delta\Theta$. This completes one RHI scan. Next, one points the Lidar in a direction orthogonal to the first RHI plane and performs another RHI scan. At the rate of 20 Hz it

is possible to complete the above described two RHI's in ≈ 72 s. Whenever possible, such a scanning mode is performed uninterruptedly, for about an hour so that, stable statistics may be obtained.

Figs. 1 and 2 are coloured graphical displays of the radial velocities during one of our RHI scannings. Red colours are Doppler velocities pointing away from the Lidar (red shift) and blue colours are when the targets are moving toward the Lidar. The full colour scale is indicated in the figures. Fig. 1 is for an RHI plane with the x-axis pointing in the direction of the surface wind and Fig 2 is in a plane normal to the first plane. In Fig. 1 the velocities are positive (red shift) when the Lidar is 5° away from the north and are negative (blue shift) when the shots are in the direction of 185°. This means that mean surface wind is essentially from the south. A low level jet at an height approximately one kilometre above the ground is also prominent. In Fig. 2 the eddy structure is apparent as well as a tendency of the wind to become more westerly with height. This latter property is revealed most prominently at the jet level where where red shifts are apparent in the positive y axis (azimuth 95°); blue shifts are recognized in the opposite direction.

4. Analysis Technique

a. Mean wind

Let α denote a radial velocity (positive if it moves away from the Lidar) and let u, v, w denote Cartesian velocities. Let x, y, z be Cartesian right handed coordinates with the positive x being in the direction of the mean surface wind. Let Θ be an elevation angle. From geometry we find,

$$\alpha = u\cos\Theta + w\sin\Theta\,;\ \text{LIDAR pointing in the direction of the mean wind}. \quad (1)$$

$$\alpha = -u\cos\Theta\ + w\sin\Theta\,;\ \text{LIDAR pointing opposite to the mean wind}. \quad (2)$$

$$\alpha = v\cos\Theta + w\sin\Theta\,;\ \text{LIDAR pointing } 90^\circ \text{ normal to the mean wind}. \quad (3)$$

$$\alpha = -v\cos\Theta + w\sin\Theta\,;\ \text{LIDAR pointing } 270^\circ \text{ normal to the mean wind}. \quad (4)$$

Assuming momentarily that u, v and w are constants at fixed height and elevation angle, it is apparent that, u and w can be found in the x-z plane while, v and w may be estimated in the y-z plane. In practice of course, u, v, and w are not constants. In that case let i be an index for observations which are constrained to be sufficiently close (say $\pm 50\,\text{m}$) to a certain height z_0 (e.g., $z_0 = 500\,\text{m}$ or $z_0 = 600\,\text{m}$ etc.). Let $\bar{u}, \bar{v}, \bar{w}$ be the ensemble average of the velocities in the above described "bin" . The average is both temporal and spatial. We may then rewrite (1), (2), (3), (4) as:

$$\alpha_i = \pm\bar{u}\cos\Theta_i + \bar{w}\sin\Theta_i + \text{fluctuations}\,;\ i = 1, 2, ..., N_1\,;\ \text{along the wind}. \quad (5)$$

$$\alpha_i = \pm\bar{v}\cos\Theta_i + \bar{w}\sin\Theta_i + \text{fluctuations}\,;\ i = 1, 2, ..., N_2\,;\ \text{across the wind}. \quad (6)$$

Here N_1 and N_2 are the number of observations in the along and across the wind "bins" respectively, corresponding to a certain height z_0. The (+) comes when the Lidar points in the positive x or positive y directions respectively. The negative sign is for negative directions.

Relations (5) define N_1 equations with two unknown $(\bar{u}, \bar{w})$ which can be solved by conventional "least square" techniques. Because only the l.h.s of (5) is known the fluctuations are omitted. For horizontally homogeneous turbulence and non-biased observations this approach may be formally justified i.e.,

$$N_1 \to \infty \Rightarrow (\bar{u}, \bar{w}) \to (\text{ensemble average of u and w}).$$

Likewise, under similar assumptions $(\bar{v}, \bar{w})$ can be found in the y-z plane.

In practice the above least square method is slightly modified. The $\bar{u}$ profile is estimated from data where most of the beams have a low elevation angle. Depending on the application two sets of $\bar{w}$ are generated, one solely from the vertically pointing beams ($\pm 2°$ away from the zenith) and, the other from inclined beams with elevation angles in the interval $30° < \Theta < 42°$.

It should also be mentioned that, at low heights most of the observations correspond to low elevation angles. In that case the estimate of $\bar{w}$ is not reliable. With the closest range being 600 m we have found that $\bar{w}$ cannot be computed reliably below 400 m. For such low heights a different method for estimating the ensemble average vertical velocity has been devised. For low elevations (say $\Theta \leq 10°$) and assuming as a rule of thumb that, $\bar{u} \gg \bar{w}$ and $\bar{v} \gg \bar{w}$, we write for a range R and an elevation Θ.

$$\alpha_i = \pm \bar{u} \cos\Theta_i + \frac{\partial \bar{u}}{\partial x} R \cos^2 \Theta_i + \text{fluctuations}\,;\; i = 1, 2, ..., N_1\,;\; \text{along wind}. \quad (7-a)$$

$$\alpha_i = \pm\bar{v}\cos\Theta_i + \frac{\partial\bar{v}}{\partial y} R\cos^2\Theta_i + \text{fluctuations}\,;\; i = 1, 2, ..., N_1\,;\; \text{across wind}\,. \quad (7-b)$$

Relation (7) and (8) may be viewed as modifications of (5) and (6), where the mean gradients are being represented explicitly rather than absorbed in the fluctuations. The mean vertical velocity for low elevations is then obtained from vertically integrating the Boussinesq's form of the mass continuity equation (e.g., Ogura and Phillips, 1962)

$$\bar{w} = \bar{w}_0 - \int_0^z (\partial\bar{u}/\partial x + \partial\bar{v}/\partial y)\,. \quad (8)$$

Here $\bar{w}_0$ is the mean vertical velocity at the surface. In this study we assume that, $\bar{w}_0 = 0$.

b. Second moments

To estimate the turbulence statistics we decompose the Cartesian velocities in the usual way as,

$$u = \overline{u} + u'\;;\; v = \overline{v} + v'\;;\; w = \overline{w} + w'\;;\alpha = \overline{\alpha} + \alpha'\,.$$

We substitute the above in (1), (2), (3), (4) and, define the mean radial velocity as,

$$\overline{\alpha} = \pm\overline{u}cos\Theta_i + \overline{w}sin\Theta_i \text{ along wind}\;;\overline{\alpha} = \pm\overline{v}cos\Theta_i + \overline{w}sin\Theta_i\,;\text{across wind}\,. \quad (9)$$

Using straight-forward algebra and the assumption of horizontal homogeneity we get for a bin corresponding to an height z_0 that,

$$\left\{ \begin{array}{l} \text{Along the wind} \\ (\alpha'^2)_i = \pm\overline{u'w'}sin2\Theta_i + \overline{w'^2}sin^2\Theta_i + \overline{u'^2}cos^2\Theta_i \; ; i = 1, 2..., N_1 \, , \\ + \text{ fluctuations.} \end{array} \right\} \tag{10}$$

And,

$$\left\{ \begin{array}{l} \text{Along the wind} \\ (\alpha'^2)_i = \pm\overline{v'w'}sin2\Theta_i + \overline{w'^2}sin^2\Theta_i + \overline{v'^2}cos^2\Theta_i \; ; i = 1, 2..., N_1 \, , \\ + \text{ fluctuations.} \end{array} \right\} \tag{11}$$

From the above it can be deduced that, the second moments $\overline{u'^2}$, $\overline{v'^2}$, $\overline{w'^2}$, $\overline{u'w'}$, $\overline{v'w'}$ can be obtained by techniques similar to the one deployed for the calculations of the mean wind i.e., a least square solution of N_1 (or N_2) equations.

Similar to the mean wind estimations (considered in the previous section) the reliability of the results depend on favourable geometries. Consequently, for each moment calculations different data stratification are used. The variance of the vertical velocity has $1/sin^2\Theta$ dependency. Therefore, at low heights (where most of the data comes from too low elevation angles) the $\overline{w'^2}$ estimate is suspect. Likewise, the horizontal momentum fluxes $\overline{u'w'}$ and $\overline{v'w'}$ have a $1/sin2\Theta$ dependency. Thus, the bulk of the observations used for estimating the momentum fluxes must come from intermediate elevations say, $30° \leq \Theta \leq 60°$. The horizontal velocities variances varies $\sim 1/cos^2\Theta$ and consequently most of the data must be at low elevations. Taking into account the above constraints as well

as the range limitations in the horizontal and vertical directions, we find that the momentum fluxes cannot be estimated reliably at heights lower than 400 m. The vertical velocity variance can be reliably estimated only from the beams which are less than 2° away from the zenith (i.e., the analysis is limited to heights greater than 600 m). The variance of the horizontal velocities on the other hand is estimated from the ground up to an height close to 2 km.

To get the vertical velocity variance at levels below 600 m one needs to integrate the continuity equation from the bottom up, setting zero vertical velocities as the lower boundary conditions. It is important to remember that only the radial winds are given. Thus, u and v are not measured at the same points. We must therefore, consider the statistical form of the continuity equation. The deterministic equation for the fluctuations is given viz.,

$$w'(z) = -\int_0^z \Big(\partial u'/\partial x + \partial v'/\partial y \Big) dz' .$$

Therefore, the vertical velocity variance is,

$$\overline{w'^2}(z) = \int_0^z \int_0^z \left[\overline{\frac{\partial u'(z')}{\partial x} \frac{\partial u'(z'')}{\partial x}} + \overline{\frac{\partial v'(z')}{\partial y} \frac{\partial v'(z'')}{\partial y}} + 2\overline{\frac{\partial u'(z')}{\partial x} \frac{\partial v'(z'')}{\partial y}} \right] dz' dz'' .$$

Assuming the turbulence to be horizontally isotropic we obtain,

$$\overline{w'^2}(z) = 2\int_0^z \int_0^z \left[\overline{\frac{\partial u'(z')}{\partial x} \frac{\partial u'(z'')}{\partial x}} \right] dz' dz'' \ ; \text{ along the mean wind.} \qquad (12)$$

$$\overline{w'^2}(z) = 2\int_0^z \int_0^z \left[\overline{\frac{\partial v'(z')}{\partial y} \frac{\partial v'(z'')}{\partial y}} \right] dz' dz'' \ ; \text{ across the mean wind.} \qquad (13)$$

In practice, instead of calculating the double integrals in (12) and (13), a computationally simpler approximate procedure is adopted. For low elevation angles,

$$\frac{1}{R}\frac{\partial}{\partial R}Rv_R \simeq \frac{\partial u}{\partial x} \; ; \text{ and } v_\Theta \simeq w \, . \tag{14}$$

Here v_Θ is the meridional velocity (i.e., the tangential velocity in the cylindrical coordinates R, Θ) and v_R is the radial velocity. Define now $\tilde{w}'$ and $\tilde{v}'_\Theta$ as the solution (with mean quantities subtracted) of the 2-D continuity equation with zero vertical velocity at the bottom namely,

$$\frac{1}{R}\frac{\partial}{\partial R}Rv'_R + \frac{1}{R}\frac{\partial}{\partial \Theta}v'_\Theta = 0 \, . \tag{15}$$

Let (as before) i be an index for a "bin" i.e., all the observations with height z_{i_k} above the ground and satisfying the condition,

$$z_{i_k} - \Delta z \leq z_i \leq z_{i_k} + \Delta z \, . \tag{16}$$

From (12)-(16) we conclude that,

$$\overline{w'^2}_i = 2/N_i \sum_{i_k=1}^{N_i} \tilde{w}'^2_{i_k} \, . \tag{17}$$

At present we are not yet able to obtain definitive vertical velocity variance from the above vertical integration method. Therefore, they will not be presented here.

c. The vertical velocity balance and the surface heat flux.

The balance of vertical velocity fluctuations for horizontally homogeneous turbulence may be shown to be (Wyngaard and Coté, 1971) as,

$$\frac{\partial}{\partial z}\left(\frac{1}{2}\overline{w'^3}\right) = -\frac{1}{\rho_o}\left(\overline{w'\frac{\partial p'}{\partial z}}\right) - \frac{\epsilon}{3} + \frac{g}{\theta_o}\overline{w'\theta'}. \qquad (18)$$

Here p' is the pressure fluctuations, ρ_o is the air density at the surface, ϵ is the kinetic energy dissipation, g is the gravity acceleration, θ_o is the potential temperature at the surface and θ' is the potential temperature perturbations. Other symbols have been defined elsewhere. Since $\overline{w'\theta'}$ is the potential temperature – vertical velocity covariance it follows that, $\rho_o C_p \overline{w'\theta'}$ is the heat flux with C_p the heat capacity of air at constant pressure.

Wyngaard and Coté (ibid.) find that under unstable conditions (i.e., positive heat flux) the pressure term at the surface layer (say the lowest 50 m of the PBL) is small compared to the other three terms in (18). Therefore, at the surface layer an estimation of the kinetic energy dissipation and the vertical gradient of the third moment of the vertical velocity would enable the calculations of the surface heat flux as a residual. It should be emphasized that the vertical velocity pressure correlation is (according to Wyngaard and Coté) an important term in the kinetic energy balance. On the the other hand at the surface layer, the correlation between the vertical velocity and the vertical pressure gradient is small compared to the other terms in (18).

Now, a traditional way to estimate the kinetic energy dissipation is by examining the line spectra of the longitudinal velocity correlation. In the inertial range the expected relation is (Batchelor, 1956),

$$\tilde{f}(\kappa) = \alpha \epsilon^{2/3} \kappa^{-5/3} . \tag{19}$$

Where κ is the wave number, α a universal constant ($= 0.5$) and $\tilde{f}(\kappa)$ the Fourier transform of the longitudinal velocity correlation (i.e., the transform of $\overline{u'(x)u'(x+r)}$ or $\overline{v'(y)v'(y+r)}$.

As has already been mentioned in the experimental design section, direct measurements of vertical velocities (from a vertically pointing beam) are available for heights greater than 600 m. This data is used to calculate the third moment of the vertical velocity $\overline{w'^3}$. For heights lower than 600 m one needs to integrate the mass continuity equation in ways similar to what have been used in the estimations of the second moments. The analogues of (12) and (13) turn out to be,

$$\overline{w'^3}(z) = 2 \int_0^z \int_0^z \int_0^z \left[\overline{\frac{\partial u'(z')}{\partial x} \frac{\partial u'(z'')}{\partial x} \frac{\partial u'(z''')}{\partial x}} \right] dz' dz'' dz''' \text{ ; along wind.} \tag{20}$$

$$\overline{w'^3}(z) = 2 \int_0^z \int_0^z \int_0^z \left[\overline{\frac{\partial v'(z')}{\partial y} \frac{\partial v'(z'')}{\partial y} \frac{\partial v'(z''')}{\partial y}} \right] dz' dz'' dz''' \text{ ; across wind.} \tag{21}$$

In practice, one does not need to evaluate explicitly the triple integrals in (20) and (21). Instead, the two dimensional continuity equation (14) with the provisions stipulated by (15) and (16) is vertically integrated. If the turbulence is horizontally isotropic we obtain,

$$\overline{w'^3}_i = 2/N_i \sum_{i_k=1}^{N_i} \tilde{w}'^3_{i_k} . \tag{22}$$

Definitive results from the above integration method are not yet available. Consequently, in this paper we limit our discussions to third moments data at heights greater than 600 m.

5. Error Analysis

a. General considerations

In the discussions below we confine ourselves to the effects observational errors have on the estimates of the mean wind and its various moments. Other error sources include inter alia, insufficiently large number of independent observations (Wyngaard, 1983) and inappropriate modelling, e.g., the turbulence may not be horizontally homogeneous. For an analysis of the vertically pointing beam data there is an additional source of error namely, a Taylor-like hypothesis which presumes that time-averaged statistics are the same as line-averaged statistics. This latter assumption is clearly dependent on the scales of motion and the averaging time; "large" eddies may move sufficiently slow and thus may not be adequately sampled. Our sample size appears to be adequate. We find for instance that, experimentations with subsets of the sample (e.g. omitting every other volume scan or every other range) have resulted in statistics which are quite close to those obtained from the complete sample ($\pm 0.1\,\mathrm{m^2 s^{-2}}$ for the second moments).

In discussing the sensitivity of the results to observational errors a distinction must be made between biased and unbiased errors as well as correlated vs. uncorrelated errors. Let β_i stands for some observation [e.g., square of the radial velocity fluctuations in (10) and (11) or the radial velocities in (5) and (6)]. Let $\delta\beta_i$ be the observational error. Let $\langle\ \rangle$ be a symbol for the expected value. The errors are considered unbiased if,

$$\langle \delta\beta_i \rangle = 0 \,. \tag{23}$$

The errors are uncorrelated (or white) if all the off-diagonal elements of the error covariance matrix are zero i.e,

$$\langle \delta\beta_i \delta\beta_j \rangle = c_{ii}\delta_{ij} \,. \tag{24}$$

Where δ_{ij} is the Kronecker delta and c_{ii} are constants.
We shall also presume lack of correlation between the exact value β_i and the error $\delta\beta_i$ i.e.,

$$\langle \beta_i \delta\beta_i \rangle = 0 \tag{25}$$

Now, for unbiased white noise it is known that, as long as the overdetermined systems of the type (5), (6), (10) or (11) are well conditioned (i.e., small changes in the r.h.s lead to small changes in the solution) the estimates become more accurate as the number of independent observations increase. Furthermore, the general "rule of thumb" is that, if $\sigma(\beta_i)$ is the standard deviation of the error of an individual observation, the error estimate of the solution is proportional to $\sigma(\beta_i)/\sqrt{N}$ where N is the number of independent observations. By contrast, when bias is present increasing the number of observations does not in general, reduce the errors. The above remarks are intuitively obvious when the estimates are of the form $\sum_i \alpha_i \beta_i$ with $\sum \alpha_i = 1$. However, their range of applicability is much broader (Jazwinsky, 1970).

The analysis becomes more involved when the errors are correlated. In fact, the simple least-square approach considered in this work is no longer optimal

(Jazwinsky, 1970). In the simple approach one tries to minimize a functional J defined as,

$$J = \sum_i \left(\sum_j a_{ij} x_j - \beta_i \right)^2 . \tag{26}$$

With a_{ij} some matrix and x_j the vector of the unknowns. In the more elaborate approach one minimizes the functional J defined as

$$J = \sum_m \sum_i \sum_s \sum_t K_{im} (a_{is} x_s - \beta_i)(a_{mt} x_t - \beta_m) . \tag{27}$$

Here K_{im} is the covariance matrix of the observational errors i.e.,

$$K_{im} = \langle \delta\beta_i \delta\beta_j \rangle . \tag{28}$$

Of course, in the special case where $K_{im} = c\delta_{im}$ (i.e., non correlated uniform observational errors) (27) is reduced to (26).

In what follows, we limit our analysis to non-correlated errors. As is shown further below the computational procedures that we have developed reduce considerably the error correlations.

While not entirely justified, we assume that, the "raw" radial velocity observations are not biased. An important source of bias for CO_2 Doppler lidars is a systematic deviations from the reference frequency. To partially overcome this problem we have eliminated all observations where the pulse monitor signal is weak or displaying a tendency toward positive or negative bias. We have also inspected the data manually. After some experimentations we have decided (subjectively) to, remove all data points where the absolute value of the radial velocity is

larger than $25\,\mathrm{ms}^{-1}$. For each beam we have computed an average and then, removed all data points whose deviations from the average exceed in absolute value $7\,\mathrm{ms}^{-1}$. Virtually identical statistics are obtained if the cutoff value is $5\,\mathrm{ms}^{-1}$. Another source of bias is pointing accuracy. Eberhard et al. (1989) discuss the (subjective) correction procedure for this type of errors.

b. Mean wind

According to Eberhard et al. (ibid.) the random error associated with an individual radial velocity estimate (using 3 shots) is $\pm 0.7\,\mathrm{ms}^{-1}$. Typically more than 2000 observations are used to estimate $\bar{u}$ and $\bar{v}$. Therefore, the uncertainty of the estimate of the mean horizontal wind due to uncorrelated non-biased observational error is quite small ($\pm 1.5\,\mathrm{cm\,s}^{-1}$).

Recall that in one method of computations the mean vertical velocity above 600 m is estimated from the vertically pointing beams. Also note (section 2) that 12 shots are fired in the vertical direction, thus the error of individual radial velocity estimate is $\pm 0.35\,\mathrm{ms}^{-1}$. The sample size in the vertical is is also quite large. If, all beams which are less than 2° away from the zenith are included we have N $\sim$ 1800. Therefore, the uncertainty of $\bar{w}$ due to non-correlated errors is $\pm 1\,\mathrm{cm\,s}^{-1}$. In another method of computations the $\bar{w}$ is estimated from data where the elevation angle is in the interval $30 \leq \Theta \leq 42$. With a smaller sample size (N=600) less favourable geometry ($\bar{\Theta} = 36$) and an uncertainty of individual measurements $\pm 0.7\ \mathrm{ms}^{-1}$, this latter method has ± 5 cm/s. On the other hand, this latter estimate may be more representative than the former.

c. Momentum flux

Let's Θ_{k_i} be a single elevation which belongs to a "bin" (i.e., a vertical layer)

k. Let m be an index for a volume scan and let v_r' be the radial velocity deviations from the mean. We can rewrite (10) or (11) as,

$$\left(v_r'^2\right)_{k_i m;1} = \overline{u'^2}\cos^2\Theta_{k_i} + \overline{w'^2}\sin^2\Theta_{k_i} + \overline{u'w'}\sin 2\Theta_{k_i}\,.\,;\text{for positive x}\,. \qquad (29)$$

And,

$$\left(v_r'^2\right)_{k_i m;2} = \overline{u'^2}\cos^2\Theta_{k_i} + \overline{w'^2}\sin^2\Theta_{k_i} - \overline{u'w'}\sin 2\Theta_{k_i}\,.\,;\text{for negative x}\,. \qquad (30)$$

Here $(;1)$ is an index for the forward beam and $(;2)$ an index for the backward beam.

Subtraction of (30) from (29) yields,

$$\overline{u'w'}_{k_i m}\,(\text{individual measurement}) = \left[\left(v_r'^2\right)_{k_i m;1} - \left(v_r'^2\right)_{k_i m;2}\right] \Big/ \left(\sin 2\Theta_{k_i}\right). \qquad (31)$$

Summing over all volume scans and all elevations within a single "bin" k one obtains,

$$\overline{u'w'}_{k}\,(\text{all measurements}) = \frac{1}{N}\sum_i \sum_m \left[\left(v_r'^2\right)_{k_i m;1} - \left(v_r'^2\right)_{k_i m;2}\right] \Big/ \left(\sin 2\Theta_{k_i}\right). \qquad (32)$$

An important point to emphasis is that, an individual $v_r'^2$ (or $\overline{v_r'^2}$) may be biased. However, due to subtraction and the homogeneity of the errors (there is

only one instrument) the flux error $\delta\overline{u'w'}$ is not. Furthermore, there is no reason to believe that, the off-diagonal terms of the error covariance matrix are not zero. In addition according to (25) little or no correlation is supposed to exist between a radial velocity error δv_r and the "true" radial velocity v_r . Under these conditions we can estimate the mean and standard deviation of $\delta\overline{u'w'}$ using conventional error analysis.

We start by noting that,

$$\delta\left(v_r'^2\right) = 2v_r'\delta v_r' + (\delta v_r')^2 . \tag{33}$$

From the error homogeneity for two different observations with indices $k,m;1$ and $k,m;2$ [see (32)] we can deduce (formally) that, an individual flux estimate is unbiased because,

$$\left\langle \delta(v_r'^2)_{k,m;1} - \delta(v_r'^2)_{k,m;2} \right\rangle = 0 . \tag{34}$$

Utilizing (33), (34) and the various non-correlation properties discussed above we obtain,

$$\left\langle [\delta(v_r'^2)_{k,m;1} - \delta(v_r'^2)_{k,m;2}]^2 \right\rangle^{1/2} = 2^{3/2}\sigma(v_r')\sigma(\delta v_r') . \tag{35}$$

Where the reader is reminded that σ is the standard deviation.

From (32)-(35) and the various error properties it is not difficult to deduce that,

$$\langle\delta\overline{u'w'}\rangle = 0 . \tag{36}$$

And,

$$\sigma(\delta\overline{u'w'}) = \left[2^{1/2}N^{-1/2}/\sin(2\overline{\Theta})\right]\sigma(v_r')\,\sigma(\delta v_r'). \tag{37}$$

Here $\overline{\Theta}$ is some mean elevation angle for the "bin" k. Since the flux retrieval is limited to elevation angles between 30° to 42° we take $\overline{\Theta} = 36°$. We assume (based on the horizontal homogeneity hypothesis) that,

$$\sigma(v_r') = \left[\overline{v_r'^2}\right]^{1/2}. \tag{38}$$

We find $\sigma(v_r') \approx \pm 2\,\mathrm{ms}^{-1}$ and from Eberhard et al. (ibid.) $\sigma(\delta v_r') = \pm 0.7\,\mathrm{ms}^{-1}$. Typical values for N are $\simeq 600$. Over all then, $\sigma(\delta\overline{u'w'}) = \pm\,0.1\,\mathrm{m}^2\mathrm{s}^{-2}$

d. Variance and third moments

As has already been indicated straight-forward squaring of the radial velocity induces bias and error correlation. Inspection of (10) and (11) reveals that the variance calculations, $\overline{u'^2}$, $\overline{v'^2}$ and $\overline{w'^2}$ do not involve subtractions. To overcome this problem we have avoided a direct squaring of the radial velocities. Instead, we have used various interpolation formulae of $v_r'^2$ whose error is unbiased. Specifically, let i be an index for either a range or an elevation let Δ be the resolution and, let α_i be some data We write,

$$(\alpha_i)^2 = \begin{cases} \alpha_i \left[\frac{2}{3}\alpha_{i+1} + \frac{2}{3}\alpha_{i-1} - \frac{1}{6}\alpha_{i+2} - \frac{1}{6}\alpha_{i-2}\right] + O(\Delta^3)\,, & \text{if r.h.s} \geq 0\,; \\ \alpha_i \frac{1}{2}\left[\alpha_{i+1} + \alpha_{i-1}\right] + O(\Delta^2)\,, & \text{if r.h.s} \geq 0\,; \\ \alpha_i\alpha_{i+1} + O(\Delta)\,, & \text{if r.h.s} \geq 0\,; \\ \alpha_i\alpha_{i-1} + O(\Delta)\,, & \text{if r.h.s} \geq 0\,; \\ \alpha_{i+1}\alpha_{i-1} + O(\Delta^2)\,, & \text{elsewhere} \end{cases} \tag{39}$$

For convenience we define,

$$\alpha_i^{int} \equiv \begin{cases} \frac{2}{3}\alpha_{i+1} + \frac{2}{3}\alpha_{i-1} - \frac{1}{6}\alpha_{i+2} - \frac{1}{6}\alpha_{i-2}\,, & \text{if (r.h.s)}\cdot\alpha_i \geq 0\,; \text{ else} \\ \alpha_i \frac{1}{2}\left[\alpha_{i+1} + \alpha_{i-1}\right]\,, & \text{if (r.h.s)}\cdot\alpha_i \geq 0\,; \text{ else} \\ \alpha_{i+1}\,, & \text{if (r.h.s)}\cdot\alpha_i \geq 0\,; \text{ else} \\ \alpha_{i-1}\,, & \text{if (r.h.s)}\cdot\alpha_i \geq 0\,; \text{ else} \\ \left[\alpha_{i+1}\alpha_{i-1}\right]/\alpha_i\,, & \text{if other tests are null} \end{cases} \tag{40}$$

Therefore, (39) is rewritten as,

$$(\alpha_i)^2 = \alpha_i^{int}\alpha_i + O(\Delta^n),\ \text{for n} \geq 1\,. \tag{41}$$

Recall now that, for the vertically pointing beam we have a spatially high resolution data in elevation ($\pm 2°$ from zenith with $0.2°$ increment). Therefore, for the vertical beam analysis the index i refers to elevation. For most parts the horizontal variance analysis is confined to elevations smaller than $20°$ and the index i then, refers to range. At any rate the error in estimating $\left(v_r'^2\right)_i$ is from (41)

$$\delta\left(v_r'^2\right)_i = \delta\left[(v_r')_i^{int}\right](v_r')_i + \delta\left[(v_r')_i\right](v_r')_i^{int} + \delta\left[(v_r')_i^{int}\right]\delta\left[(v_r')_i\right] + O(\Delta^n)\,. \quad (42)$$

It is worth noting that,

$$\left\langle \delta(v_r')_i \delta(v_r')_i^{int} \right\rangle = 0 \text{ but } ; \langle \delta(v_r')_i \delta(v_r')_i \rangle \neq 0\,. \quad (43)$$

It is apparent from (39)-(43) and the fact that the errors should not be correlated with the "exact values" that, using the approximate form for the square of the radial velocity would result in an unbiased errors i.e.,

$$\left\langle \delta(v_r'^2)_i \right\rangle = 0 + O(\Delta^n)\,, \text{ for } n \geq 1 \quad (44)$$

The error covariance matrix of $\delta\left(v_r'^2\right)_i$ can also be calculated. While the flux errors covariance matrix is diagonal this latter quantity is not, because, the interpolation induce correlations. However, the matrix is still quite sparse. Each observational error is correlated only with its two immediate neighbours. Further more, a straight forward calculation of the error correlation between two adjacent neighbours, and utilizing the various remarks about correlation (or lack of it) between various quantities would reveal that these off-diagonal terms are smaller than the diagonal one by a factor of $\frac{1}{9}\,\mathrm{cor}\left[(v_r')_i (v_r')_{i+1}\right]$. Where cor [ ] is the correlation coefficient (≤ 1) between two neighbouring observations. Therefore, we proceed with error analysis ignoring the effects of the off-diagonal terms.

Regarding the standard deviations of $\delta\left(v_r'^2\right)$ we utilize (40) – (44) and the supposed lack of correlation between errors and "exact" observations (25) to find that for an individual measurements,

$$\sigma(\delta v_r'^2) = 2\sigma(v_r')\sigma(\delta v_r')\,. \tag{45}$$

And for N measurements,

$$\sigma(\delta v_r'^2) = \left(2/N^{1/2}\right)\sigma(v_r')\,\sigma(\delta v_r')\,. \tag{46}$$

We can apply (46) directly to find (for vertically pointing beams) the standard deviation of the error of the vertical velocity variance namely,

$$\sigma(\delta\overline{w'^2}) = \left(2/N^{1/2}\right)\sigma(v_r')\,\sigma(\delta v_r')\,;\ \text{for the vertical beam}\,. \tag{47}$$

We can take $\sigma^2(v_r') = \overline{w'^2} \approx 1\ \mathrm{m^2 s^{-2}}$. As has already been indicated in the experimental design section for the vertically pointing beam we have, $\sigma(\delta v_r') = \pm 0.35\ \mathrm{ms_1}$. For a single volume scan we have 40 observations which are only $\pm 2°$ away from the zenith; we have 45 volume scans so that $N = 1800$. Overall then $\sigma(\delta\overline{w'^2}) = \pm 0.016\ \mathrm{m^2 s^{-2}}$; a rather small number.

Similar considerations can be used to estimate the errors in the third moments of the vertical velocity with the result that,

$$\sigma(\delta\overline{w'^3}) = (3/N^{1/2})\overline{w'^2}\sigma(\delta v_r')\,. \tag{48}$$

Substituting appropriate values we get $\sigma(\delta\overline{w'^3}) = 0.024\,\mathrm{m^3 s^{-3}}$.

We can also apply (46) to estimate the error in the horizontal wind variance. The following considerations are pertinent:

First for heights larger than 600 m one can append the l.h.s of (10) and (11) by

the vertical velocity variance obtained from the vertically pointing beam. Second, for heights less than 600 m the horizontal variance analysis can be constrained so that observations with an elevation angle greater than 20° are excluded. For a 600 m height this means that elevations in the interval $5.74° \leq \Theta \geq 18°$ are included. If we neglect the vertical velocity variance contributions in (10) or (11) the bias will be in the order of $\overline{w'^2}\sin^2\left(\frac{1}{2}(18+5.74)\right)$. For vertical velocity variance in the order of $1\,\mathrm{m^2 s^{-2}}$ we get a small bias of the order of 4 cm/s. Third, by adding (30) to (29) we can eliminate the momentum flux from the equations. Taking the above into account we can follow steps similar to (31) − (37) and obtain, that

$$\sigma(\delta\overline{u'^2}) = \left[2^{1/2}N^{-1/2}/\cos^2(\overline{\Theta})\right]\sigma(v_r')\,\sigma(\delta v_r')\,. \tag{49}$$

Likewise,

$$\sigma(\delta\overline{v'^2}) = \left[2^{1/2}N^{-1/2}/\cos^2(\overline{\Theta})\right]\sigma(v_r')\,\sigma(\delta v_r')\,. \tag{50}$$

Typical values for N in the horizontal variance analysis are in the order of 4000 for low heights to 2000 for $z \sim 1.5\,\mathrm{km}$. We take $\bar{\Theta} \approx 10$, $\sigma(\delta v_r') = 0.7\,\mathrm{ms^{-1}}$ and $\sigma(v_r') = 2\ \mathrm{ms^{-2}}$ and obtain that, $\sigma\Big(\delta(\text{horizontal variance})\Big) \sim 0.05\,\mathrm{m^2 s^{-2}}$

To test the effect of the interpolation formula (39) we have conducted experiments comparing the use of (39) vs. straight forward squaring. We find, that the momentum flux estimates are not sensitive to such variations. This is in line with the finding of the previous section where, we have shown that the flux estimate is not biased. By contrast employing (39) have resulted in variance reduction of the order of $1 - 2\ \mathrm{m^2 s^{-2}}$.

6. Principal Features

a. Mean properties

Using our analysis technique we find that the mean surface wind is essentially from the south (direction $\sim 185°$). We have chosen a right-handed Cartesian coordinate system such that, the positive x-axis is the direction of the mean surface wind. We call the x-component of the wind u and the y-component v. The dependence of $\bar{u}$ in height for the two case studies is shown in Fig. 3. The wind at the lowest 500 m appears to be well mixed; a southerly jet is prominent at $\sim$ 1 km. The dependence of $\bar{v}$ in height is shown in Fig. 4. By construction $\bar{v}$ is zero at the surface. It is becoming more westerly with height up to an height of $\sim$ 0.9 km for the earlier sounding and $\sim$ 1.1 km for the later sounding, then becoming more easterly (at 1.3 km and 1.5 km respectively) where it turns more westerly again. All the above features are in good agreement with hourly releases of rawinsonde (Brutsaert, FIFE Document, ABL-1). In Fig. 5 we present potential temperature soundings (Brutsaert, ibid.) starting at 15:45, 16:59 and 18:54 UTC respectively (i.e., before, during and after our Lidar measurements). The growth of the mixed layer (i.e., the region where the lapse rate is close to adiabatic) during the two hour period is apparent. An exact definition of the "top" of the mixed layer is difficult. By one criteria we can place the "top" to be at 700 m for the first two soundings and, at 1.3 km for the last one. By another criteria one may place the top at 0.7 km, 1 km and 1.3 km respectively; more in line with traditional mixed-layer models of the type discussed by Tennekes (1973).

The mean vertical wind is displayed in Fig. 6. One profile is derived using only the vertically pointing beam data. The second profile is estimated from data where the elevation angle is in the neighbourhood of $30 \leq \Theta \leq 42$. This latter pro-

file is used to define the mean radial velocities (9) and the fluctuations needed for the momentum flux calculations (32). While, the $\bar{w}$ estimate from the vertically pointing beams are less prone to observational errors, the statistics of the inclined beam may be more representative. It is reassuring to find essentially zero vertical velocities above the mixed layer. The unusually large mean vertical motion in the mixed layer is perplexing. It could be due to deficiencies of the Taylor hypothesis. Thus, long term sampling (1 hr) of the vertically pointing beam data may not adequately represent the eddies that are either too slow or too large. We have also attempted to obtain mean vertical motion by vertically integrating the continuity equation from the bottom up [(7-a), (7-b), (8)]. While the integration reveals negative motions at the lowest 600 m there is still no satisfactory matching at 600 m between the vertical integration result and the vertically pointing beam data.

b. Momentum fluxes

The vertical profiles of $\overline{u'w'}$ are shown in Fig. 7 and, those of $\overline{v'w'}$ are displayed in Fig 8. At the mixed layer the sign of the fluxes are in agreement with the eddy viscosity concept, i.e.

$$\overline{u'w'} = -K_1 \partial \bar{u}/\partial z\,; \quad \text{and}\,; \quad \overline{v'w'} = -K_2 \partial \bar{v}/\partial z\,; \quad \text{with;} \quad (K_1, K_2) > 0\,.$$

The above is true provided that, the shear is interpreted not locally but, as some kind of vertical average from the surface layer to the top of the mixed layer. Taking local values of the shear may lead to unrealistically large values of K_1 and K_2 when the wind does not change with height (Figs. 3 and 4).

In the mixed layer the $\overline{u'w'}$ values are negative; near the surface this implies retardation of the surface wind. The values of $\overline{v'w'}$ on the other hand are posi-

tive; this implies retardation of the (negative) $\bar{v}$ component (Fig. 4). For comparison purposes we also display in Fig. 7 the aircraft estimate of $\overline{u'w'}$ at $z = 50$ m (McPherson et al., FIFE document, ABL-6). The Lidar and aircraft values are consistent even though the lowest level where Lidar derived fluxes are feasible is 450 m. It should also be mentioned that with the exception (noted further below) the flux values are insensitive to the method by which $\bar{w}$ is calculated. The present results are obtained by using the $\bar{w}$ estimated from the inclined beams data ($30° \leq \Theta \leq 42°$) data and then, subtracting it (and the mean horizontal wind) from the radial velocities. But, similar results are obtained if $\bar{w}$ is estimated from data where the beams are vertically pointing ($\pm 2°$). The only exception is that, for the 16:11-17:11 UTC period a local minima (not shown here) is indicated around z=800 m if $\bar{w}$ is estimated from vertically pointing beam data whereas, none seems to be apparent (Fig. 7) if the present $\bar{w}$ is used.

The flux values of $\overline{u'w'}$ in the stable layer above the jet do not support the eddy viscosity concept; it continues to be negative even though the wind above the jet is decreasing with height. Furthermore, unusually large values are observed for both case studies (e.g., $\overline{u'w'} \approx -2.5$ m^{2}s^{-2} at z ≈ -1.4 km for the 17:29-18:20 UTC case study). To get further insight on the nature of the perturbations we have examined time series of the vertically pointing beam data at various observational levels (600 m $\leq$ z $\leq$ 1950 m). The time resolution is 36 s. Fig. 9 displays the time series for the period 17:29-18:20 UTC. Fig. 10 is the spectral analysis of Fig. 9. In the stable layer (say z $\geq$ 800 m) the spectra has two distinct peaks; one with period T=54 min (the first Fourier mode) and the other with period of 10.8 min (the fifth Fourier mode). The significance of the first Fourier mode is not clear. According to standard time series analysis (e.g., Jenkins and Watts, 1968) the spectral amplitude of the first Fourier mode

may be influenced by artifacts such as the method of detrending, an inadequate sampling, the assumption of periodicity, etc. The peak of the fifth Fourier mode (10.8 min) is deemed not to be susceptible to the above artifacts. It is interesting that the 10.8 minutes period correspond to an angular frequency ($\omega = 2\pi/T$) of the order of 10^{-2} s^{-1}, not too far from the standard atmospheric value for the Brunt Väisälä frequency $\left[(g/\theta)(\partial\theta/\partial z)\right]^{1/2}$. A spectral peak at the Brunt Väisälä frequency has also been reported in numerous other studies of vertical velocity spectra of stable atmospheres (e.g., Ecklund et al., 1986; Gage, 1990). From the wind and temperature sounding we have also estimated the Richardson number R_i defined viz.,

$$R_i = \frac{(g/\theta)(\partial\theta/\partial z)}{(\partial u/\partial z)^2}. \tag{51}$$

In the stable layer we have found that, the Richardson number is in the range of 1-2; significantly above the critical Richardson number (=1/4) below which turbulence is dominant. Furthermore, a Richardson number greater than unity is a necessary condition for waves absorption at critical layers.

At present we interpret the large counter-gradient fluxes as a manifestation of the interactions between the convection in the mixed layer and waves in the stable layer. In particular, for reasons discussed further below we believe that the large fluxes are related to the existence of a so called "critical layer". Previous studies (Kuetner et al., 1987 and Clark et al., 1986) have already identified the convection in the mixed layer as an important energy source for waves in the troposphere. To further proceed, let us examine the equation that describes the vertical structure of two dimensional linear gravity waves in a stable atmosphere is (e.g., Gossard and Hooke, 1975 p. 456)

$$W_{zz} + \left[\frac{N^2}{(c-\bar{u})^2} + \frac{\bar{u}_{zz}}{(c-\bar{u})} - k^2\right] W = 0\,. \tag{52}$$

Here c is the speed of the wave, W is the amplitude of the vertical wave velocity and k is the angular wave number ($c = \omega/k$; with ω the angular frequency). Differentiation with respect to z is denoted by a subscript z and other symbols have been defined above. If a situation occurs where, the mean wind ($\bar{u}$) at a layer of height z is equal to to the speed of the wave then, that layer is termed "critical layer". Mathematically the differential equation (52) becomes singular.

A detailed quantitative discussion of critical layers is beyond the scope of this paper but few remarks are in order. When a wave reaches a critical layer and the Richardson number is greater than 1, the wave energy is presumed to be completely absorbed. Even if (due to say non-linear effects) reflection does occur its effect must be limited since, the wave can not significantly penetrate into the adiabatic layer below. Overall then, if the predictions of linear theory are qualitatively correct the presence of a critical layer should result in a build-up of wave energy and momentum in that layer. Of course, once the wave amplitude grows non-linear effects take place. As long as the flow can be characterised by a single frequency (e.g. the Brunt Väisälä frequency) the effect of the non-linearity is to steepen the wave front* and to diminish the gradients at the back. This should enhance the "downward" transport at the front and diminish the "upward" transport in the back so that on the average the "downward" transport is enhanced. Another consequence of non-linearity is the breakdown of the so called Eliassen and Palm flux theorem which states that for linear gravity waves $\partial/\partial z(\overline{u'w'}) = 0$.

* Here "front" and "back" are defined in a frame of reference moving with the mean wind; the terms "upward" and "downward" are used in the context of a right-handed coordinate system with the x-axis pointing in the direction of $c - \bar{u}$.

Our data (Fig. 7) indicate large momentum flux divergence.

To precisely establish the existence (or lack of) a critical layer one needs to independently measure the mean wind and the group velocity of the wave. This latter measurements are not feasible with the present scanning. Therefore, the above discussions must be regarded as speculative; however, if one accepts the proposition that the energy source is the PBL convection and, the Brunt Väisäl"a frequency is dominant, then it is possible to establish a bound for the phase velocities and see whether they are in a range which can overlap with that of the mean wind. From our spectra of the horizontal velocities (Figs 15 and 16) we have inferred that, the horizontal scales of the energy containing eddies in the PBL are in the range of at least 600 m - 6 km. This should excite waves in the stable layer with wave length λ also in that range. Taking the Brunt Väisälä frequency N to be $\sim\ 10^{-2}\,\mathrm{s}^{-1}$ we get (from $c = \omega/k$ and $k = 2\pi/\lambda$) that the phase velocities are in the range of $1\,\mathrm{ms}^{-1} - 10\,\mathrm{ms}^{-1}$. From Fig. 3 (the mean $\bar{u}$ wind) we establish that the velocities in the stable layer are in range of $8\,\mathrm{ms}^{-1}$ to $19\,\mathrm{ms}^{-1}$ with an indication of further decrease with height. Thus, an existence of a critical layer seems plausible. We suspect that such critical layers may be present in other cases where, the Richardson number is above unity and, the energy containing eddies in the mixed layer have lengths scales large enough, to excite waves whose phase velocities are comparable to the mean wind aloft.

c. Variance

The vertical profile of the variance of w $\overline{w'^2}$ is shown in Fig. 11. We have used the vertically pointing beam for these calculations. Only the 17:29 - 18:20 UTC is shown here because of some uncertainties in the pointing accuracy of the vertically pointing beam for the earlier time. The variance gener-

ally decreases with height but a relative maxima near the critical layer is observed. Because vertically pointing data is not available at heights less than $\sim 0.5z_i$; (z_i the height of the mixed layer), the well known maxima at $\sim (0.2z_i - 0.4z_i)$ is not detected.

The vertical profiles of the variance of u ($\overline{u'^2}$) is shown in Fig. 12 and that of of $\overline{v'^2}$ is displayed in Fig. 13. For most part the profiles are consistent with the established conceptual picture of the PBL (e.g., Caughey, 1984). In the surface layer the variance is decreasing with height; in the mixed layer the horizontal variances seems to be well mixed as well. A notable departure from classical results is in the vicinity of presumed critical levels. The horizontal variances seems to have local maximas when, local maximas of absolute values of momentum fluxes are present. In the part of the stable layer above the critical layer, the fluxes diminish with height in agreement with other observations of the stable layer (e.g., Lenschow et al. 1989). The variance of u also diminishes with height at the top of the domain, but the v variance does not. This latter phenomenon is probably associated with the transient nature of the v wind in that region (Fig. 4). Later soundings (not shown here) has revealed that the v wind (approximately east-west in the present coordinates) to be consistently more westerly with height.

d. The kinetic energy dissipation, and the surface heat flux.

Recall from the discussions in section (4. c) the balance equation for the vertical velocity fluctuations in the form (18) rewritten here as (53) viz.,

$$\frac{\partial}{\partial z}\left(\frac{1}{2}\overline{w'^3}\right) = -\frac{1}{\rho_o}\left(\overline{w'\frac{\partial p'}{\partial z}}\right) - \frac{\epsilon}{3} + \frac{g}{\theta_o}\overline{w'\theta'}. \qquad (53)$$

As has already been discussed the pressure term may be neglected near the surface therefore, the heat flux may be calculated as a residual balance between the the gradients of the third moments and the kinetic energy dissipation ϵ. Recall also that, the kinetic energy dissipation can be estimated from the spectra and (19) provided that an inertial $\kappa^{-5/3}$ law is established.

Fig. 14 is a profile of the third moments of the vertical velocity $\overline{w'^3}$. The positive values at heights $600\,\mathrm{m} \leq z \leq 800\,\mathrm{m}$ is encouraging. On the other hand the negative values up to an height of 1200 m are perplexing. If it is real it could be due to the steepening of the waves or the or skewed negative motions in the entrainment zone. On the other hand it could be due to sampling; and the inadequacy of relating turbulence parameters to the statistics of time series in a single spatial location.

Figs. 15 and 16 are the longitudinal spectra of the u and v velocity correlation in the surface. All the beams in the lowest 100 m of the domain are included. Each beam is spectrally analysed and than all the spectras in the entire time period (17:29 - 18:20) are combined. Prior to evaluating the Fourier coefficients the data is subjected to an high pass filter to remove wave length larger than 5.4 km. To minimize aliasing a low pass filter with weights (1/4, 1/2, 1/4) is also applied. This removes all wavelength shorter than 2Δ, where Δ is the range resolution. In both the u and v spectra an inertial -5/3 power law is clearly established. As the wave lengths get shorter, some attenuation due to the application of the low pass filter is apparent. The saturation at the high wave numbers is almost surely due to noise.

From the amplitude of the power spectra at the inertial range we have estimated that $\epsilon = 5.02 \times 10^{-3}\,\mathrm{m^2 s^{-3}}$. By assuming that $\overline{w'^3}(z = 0) = 0$ and, using the next two data points in Fig. 14 to fit a parabola we obtain

$\frac{1}{2}\frac{\partial \overline{w'^3}}{\partial z}(z = 25\,\mathrm{m}) = 1.43 \times 10^{-3}\,\mathrm{m^2 s^{-3}}$. From this and using $\rho_0 = 1.275\,\mathrm{kg\,m^{-3}}$, $C_p = 1004\,\mathrm{J\,deg^{-1}\,kg^{-1}}$ and $\theta_0/g = 30\,\mathrm{deg\,s^2\,m^{-1}}$ we get a surface heat flux value $\sim 100\,\mathrm{Wm^{-2}}$. This is in apparent agreement with the average estimate of the surface stations. Nevertheless (as discussed above) the contribution from the gradient of the third moments is uncertain.

6. Conclusions

1. With respect to the analysis technique we have shown that for an horizontally homogeneous turbulence the mean wind, its variance and the vertical momentum fluxes can be deduced from a single Doppler Lidar data. While the accuracy of individual radial velocity is only $\pm 0.7\ \mathrm{ms^{-1}}$ we have exploited the large sample size to reduce the errors considerably. For the purpose of estimating the first moments the error reduction is in essence a simple averaging procedure. In calculating higher moments non-linear effects usually modify the error field so that it becomes biased and correlated. Under these circumstances simple averaging does not reduce the error's variance. We have developed effective procedures to remove bias and reduce error correlation. Taking into account the large sample size we have shown that if the above mentioned procedures are utilized, we can obtain estimates of the variance and momentum fluxes with sensitivity to observational error which is at most $\pm 0.10\ \mathrm{m^2 s^{-2}}$. Regarding hardware improvements, the most serious problem is the stability of the reference frequency. Another serious limitation is the range resolution (=150 m). For PBL studies a more desirable resolution is 25 m. New solid state Doppler Lidars could address both issues and are currently under developments in WPL and elsewhere.
2. Spectral analysis of the horizontal velocities has in a natural way produced a

$\kappa^{-5/3}$ power law at the inertial range. We view this as another indication of the viability of our analysis technique. From the power spectrum we have deduced the kinetic energy dissipation. Using the statistical form of the Navier-Stokes equation the surface heat flux has been derived as a residual balance between the kinetic energy equation and the vertical gradient of the third moment of the vertical velocity. Our estimate of the surface heat flux is consistent with the average estimate of the surface stations. This latter result must be considered preliminary, because at present, the third moment of the vertical velocity cannot yet be reliably estimated at heights which are below 600 m.

3. The momentum fluxes in the mixed layer are in qualitative agreement with the eddy viscosity concept. However, in the stable layer the fluxes are counter-gradient. The Brunt Väisälä frequency is the dominant one in the stable layer and the Richardson number is greater than one. We view this as an indication that the transport is accomplished by gravity waves. In the stable layer negatively large flux values ~ -1.5 m^{2}s^{-2} are concentrated in thin layers where also, the flux divergence is large; in contradiction to the Eliassen-Palm flux theorem which, predicts (in the linear case and in the absence of sources or sinks) that the flux divergence is null. Our interpretation of the large flux values is that they are due to an absorption by a critical layer and the non-linear effect of steepening of gravity waves.

ACKNOWLEDGMENTS

This work is supported by NASA/NSF grant ATM 8617735 and by NASA grant NAG 5-1379 awarded to Oklahoma university. We appreciate the unselfish cooperation of Wilfried Brutsaert in supplying to us the balloons sounding. We

thank I. MaCpherson and R. Desjardins for providing us with the aircraft estimate of the momentum flux. We recognise gratefully discussions with R. Rotuno on the fundamentals of gravity waves. We are indebted to F. Hall and P. Sellers for their continuous encouragement and support. Critical comments on an early version of this manuscript by G. Wilks have resulted in substantial improvements.

REFERENCES

Batchelor, G. K., *The Theory of Homogeneous Turbulence,* 197 pp., Cambridge University Press, London, 1956.

Caughey, S. J., Observed characteristics of the atmospheric boundary layer, in *Atmospheric Turbulence and Air Pollution Modelling,* edited by F. T. M. Nieuwstadt, and H. Van Dop, pp. 107-158, Reidel, Dordrecht,1984

Clark, T. L., T. Hauf and J. P. Kuettner, Convectively forced internal gravity waves: Results from two-dimensional numerical experiments, *Q. J. R. Meteorol. Soc.*, **112**, 899-925, 1987

Eberhard, W. L., R. E. Cupp and K. R. Healy, Doppler Lidar measurements of profiles of turbulence and momentum flux, *J. Atmos. Ocean. Technol.*, **6**, 809-819, 1989.

Ecklund, W. L., K. S. Gage, G. D. Nastrom and R. G. Balsley, A preliminary climatology of the spectrum of vertical velocity observed by clear-air Doppler Radar, *J. Clim. and App. Meteor.*, **7**, 885-892, 1986.

Gage, K. S., Radar observations of the free atmosphere: Structure and dynamics, in *Radar in Meteorology,* edited by D. Atlas, pp. 534-565, Amer. Meteor.

Soc., Boston, 1990.

Gossard, E. E. and W. H. Hooke, *Waves in the Atmosphere,* 456 pp., Elsevier, New York, 1975.

Jazwinski, A. H., *Stochastic Processes and Filtering Theory,* 376 pp., Academic Press, NY., 1970.

Jenkins, J. M., and D. G. Watts, *Spectral Analysis and its Application,* 523 pp., Holden-Day, San Francisco, 1968

Kropfli, R. A., Single Doppler Radar measurements of turbulence profiles in the convective boundary layer, *J. Atmos. Ocean. Technol.,* **3**, 305-313, 1986.

Kuetner, J. P., P. A. Hildebrand and T. L. Clark, Convection waves: Observations of gravity wave systems over convectively active boundary layers, *Q. J. R. Meteorol. Soc.,* **113**, 445-467, 1987.

Lenschow, D. A., X. S. Li, C. J. Zhu and B. Stankov, The stably stratified boundary layer over the great plains, *Boundary Layer Meteor.,* **42**, 95-121, 1987.

Lilly, D. K., Mesoscale variability of the atmosphere, in *Mesoscale Meteorology - Theories, Observations and Models,* edited by D. K. Lilly and T. Gal-Chen, pp. 13-24, Reidel, Dordrecht, 1983.

Ogura, Y., and N. A. Phillips, Scale analysis of deep and Shallow convection in the atmosphere, *J. Atmos. Sci.,* **19**, 173-179, 1962.

Tennekes, H., A model for the dynamics of the inversion above a convective boundary layer, J. Atmos. Sci., **30**, 558-567, 1973.

Wyngaard, J. C., Lectures on the Planetary Boundary Layer, in *Mesoscale Meteorology - Theories, Observations and Models,* edited by D. K. Lilly and T. Gal-Chen, pp. 603-650, 1983.

Wyngaard, J. C., and O. R. Coté, The budgets of turbulence kinetic energy and temperature variance in the atmospheric surface layer, *J. Atmos. Sci.,* **28**, 190-201, 1979.

FIGURE CAPTIONS

Fig. 1 RHI display in the direction of the mean surface wind. Note the southerly jet at 1 km. Refer to text for further explanations.

Fig. 2 RHI display in the direction normal to the mean surface wind. Note the eddy structure in the mixed layer. Also, the wind becomes more westerly with height.

Fig. 3 Profiles of $\bar{u}$ with height for the two case studies. A right handed coordinate system is used such that the positive x-axis is the direction of the surface wind. The surface wind direction at 17:29-18:20 UTC period is ~185° while the direction at the other period is ~189°.

Fig. 4 Profiles of $\bar{v}$ with height for the two case studies. Note by construction $\bar{v}$ =0 at the surface. Refer to Fig. 3 and the text for further explanations.

Fig. 5 Vertical profiles of θ (the potential temperature) from nearby balloon measurements at 15:45, 16:59 and 18:54 UTC, before, during and after our measurements period. Courtesy of W. Brutseart.

Fig. 6 Vertical profiles of $\bar{w}$ with height for the period 17:29-18:20 UTC. One profile is obtained using the vertically pointing beams and the other from inclined beams.

Fig. 7 $\overline{u'w'}$ profiles for the two case studies. Refer to Figs.3, 4 and the text for explanations of the coordinate system. The aircraft data is for 17:29-18:20 UTC (Courtesy of R. Desjardins and I. MacPherson).

Fig. 8 $\overline{v'w'}$ profiles for the two case studies. Refer to Fig. 3 and the text for explanations of the coordinate system.

Fig. 9 Time series of the vertically pointing beam Doppler velocities for various heights and for the period 17:29-18:20 UTC. The horizontal axis is time in hour. The time resolution is 36 s. The amplitude in ms^{-1} is indicated on the vertical axis, while height is indicated by a series of horizontal lines.

Fig. 10 Spectral analysis of Fig. 9. The periods T_n (in minutes) are indicated in the horizontal axis. Also indicated is the Fourier mode $n=T/T_n$ with T the longest resolvable period (=54 min).

Fig. 11 Vertical profile of the variance of w ($\overline{w'^2}$) with height for the period 17:29-18:20 UTC.

Fig. 12 Vertical profile of the variance of u ($\overline{u'^2}$) with height for the periods 16:11-17:10 UTC and 17:29-18:20 UTC. Refer to Fig.3 and the text for explanations of the coordinate system.

Fig. 13 Vertical profile of the variance of v ($\overline{v'^2}$) with height for the periods 16:11-17:10 UTC and 17:29-18:20 UTC. Refer to Figs.3, 4 and the text for explanations of the coordinate system.

Fig. 14 Profile of the third moment of the vertical velocity $\overline{w'^3}$ derived from the vertically pointing beams. The observation period is 17:29-18:20 UTC.

Fig. 15 Longitudinal spectra of the u velocity correlation at the surface. $\kappa=n2\pi/\lambda_{max}$; $n=1,2,...,N$. λ_{max} is the longest resolvable wavelength (=5.4 km) $N=\lambda_{max}/\Delta$ with Δ=150m, Δ is the spatial resolution. The -5/3 fit is also indicated.

Fig. 16 Longitudinal spectra of the v velocity correlation at the surface. Refer to Fig. 15 for explanations. The -5/3 fit is also indicated.

3

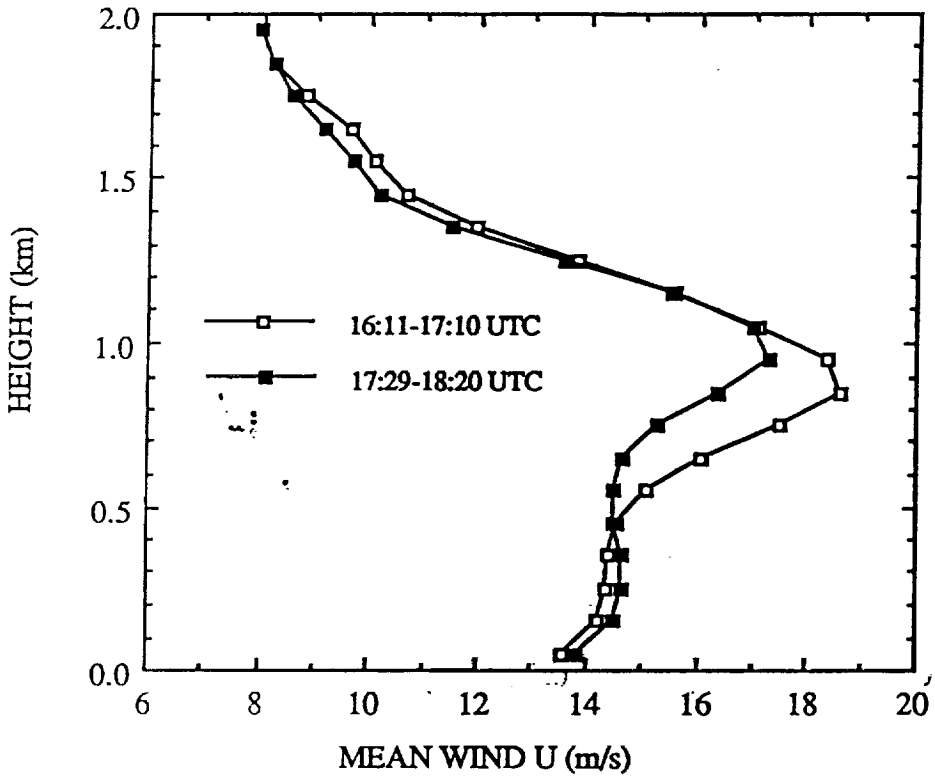
2.0
1.5
1.0
0.5
0.0
HEIGHT (km)
16:11-17:10 UTC
17:29-18:20 UTC
6
8
10
12
14
16
18
20
MEAN WIND U (m/s)

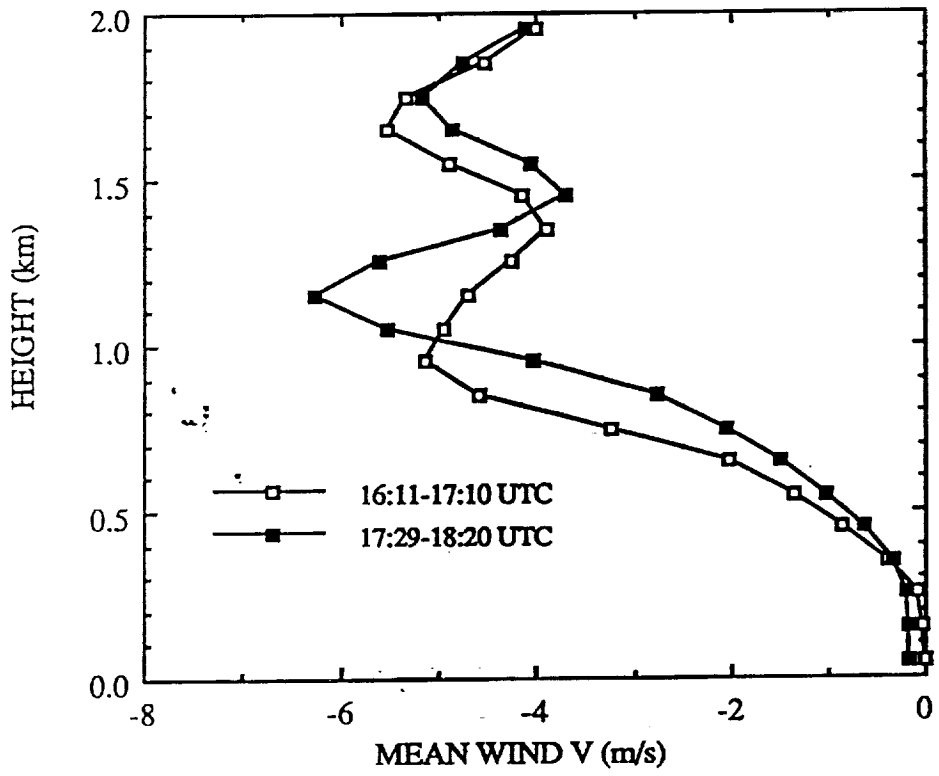
2.0
1.5
1.0
0.5
0.0
HEIGHT (km)
-8
-6
-4
-2
0
MEAN WIND V (m/s)
16:11-17:10 UTC
17:29-18:20 UTC

5

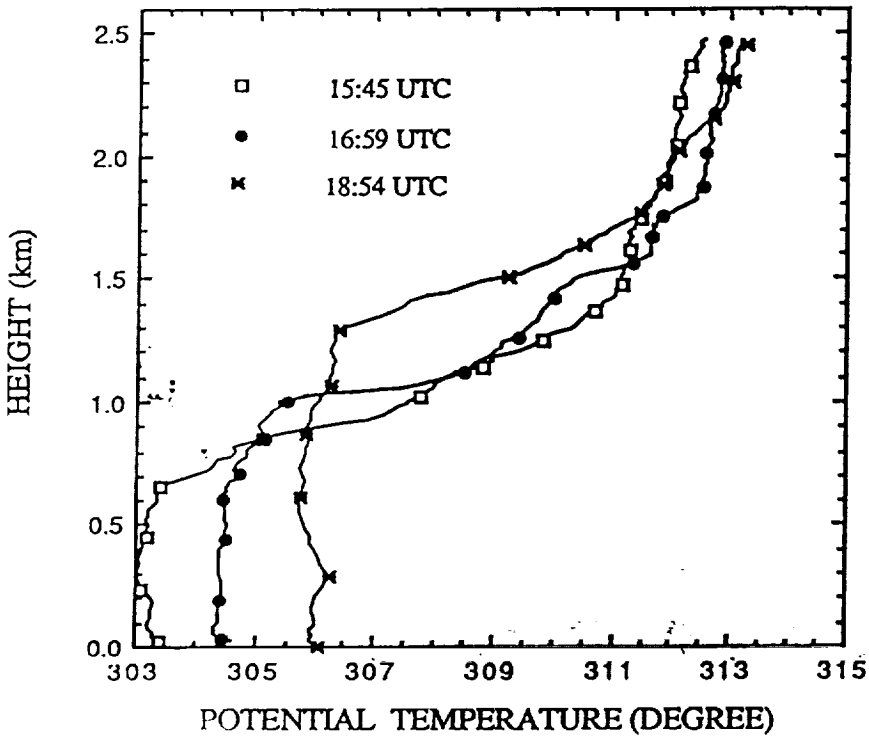
15:45 UTC
16:59 UTC
18:54 UTC
HEIGHT (km)
2.5
2.0
1.5
1.0
0.5
0.0
303
305
307
309
311
313
315
POTENTIAL TEMPERATURE (DEGREE)

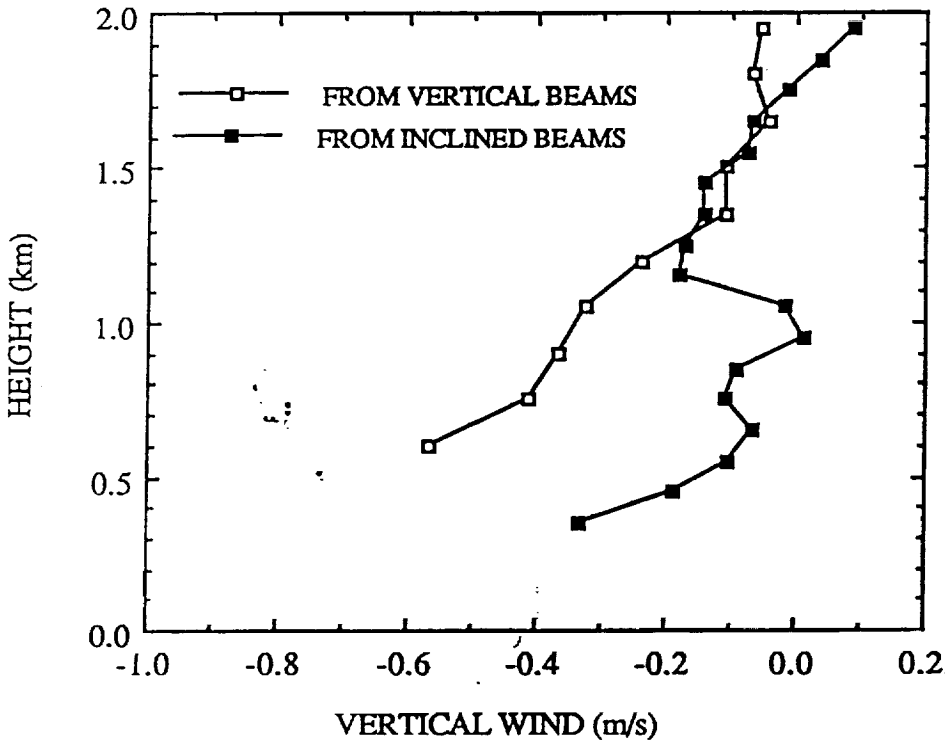
FROM VERTICAL BEAMS
FROM INCLINED BEAMS
HEIGHT (km)
2.0
1.5
1.0
0.5
0.0
-1.0
-0.8
-0.6
-0.4
-0.2
0.0
0.2
VERTICAL WIND (m/s)

7

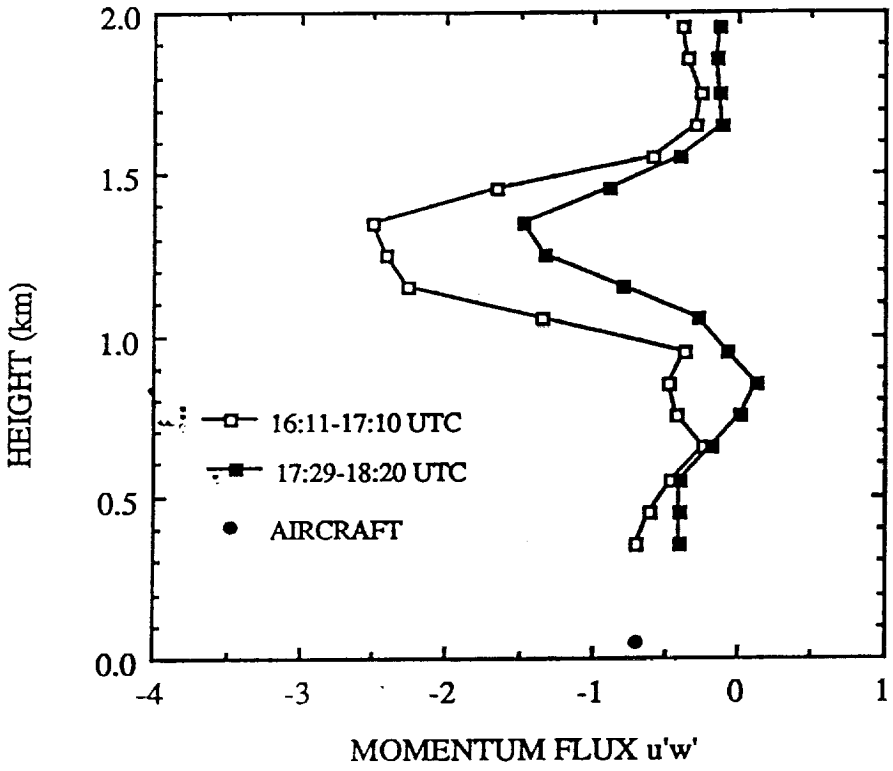
2.0
1.5
1.0
0.5
0.0
HEIGHT (km)
16:11-17:10 UTC
17:29-18:20 UTC
AIRCRAFT
-4
-3
-2
-1
0
1
MOMENTUM FLUX u'w'

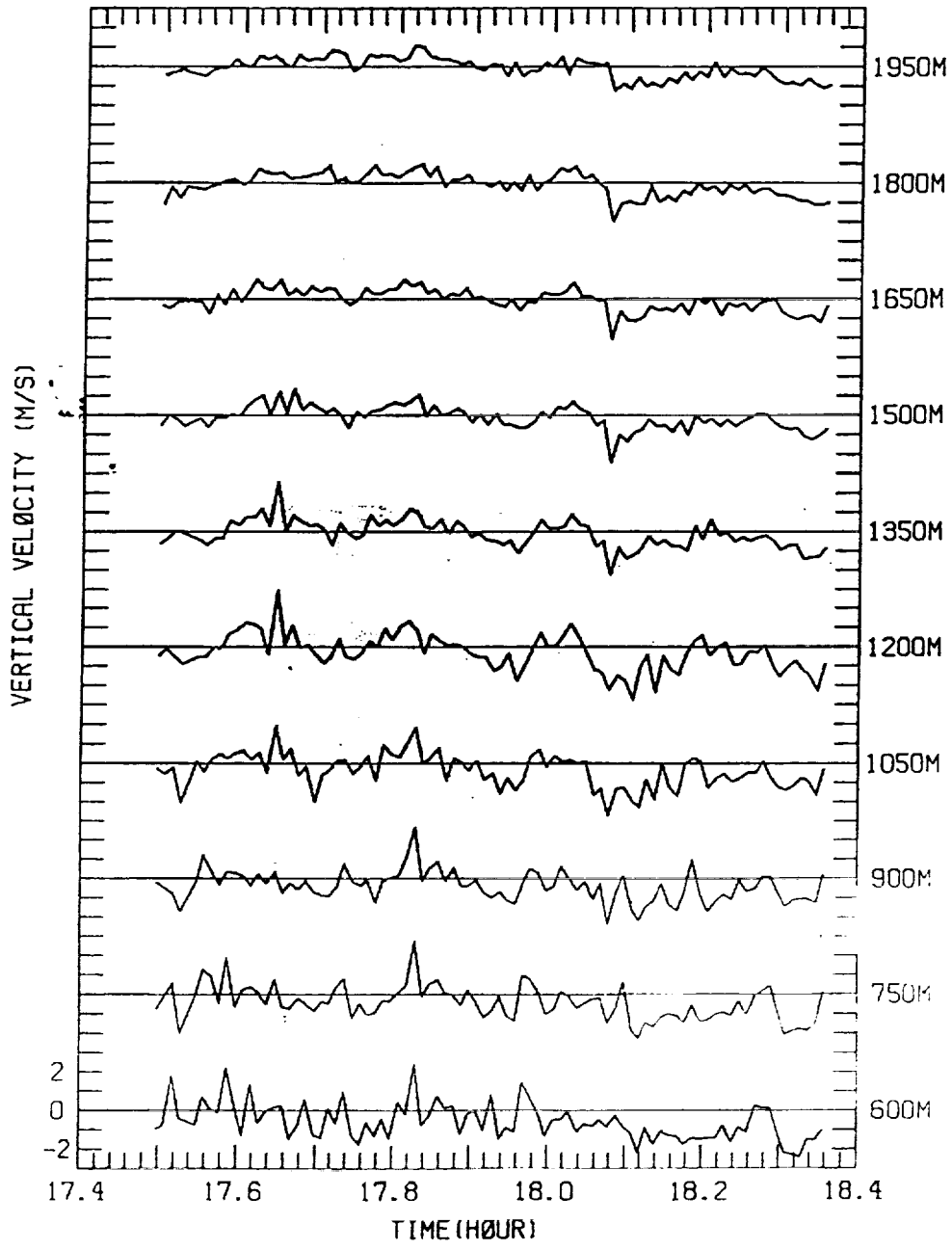

10.

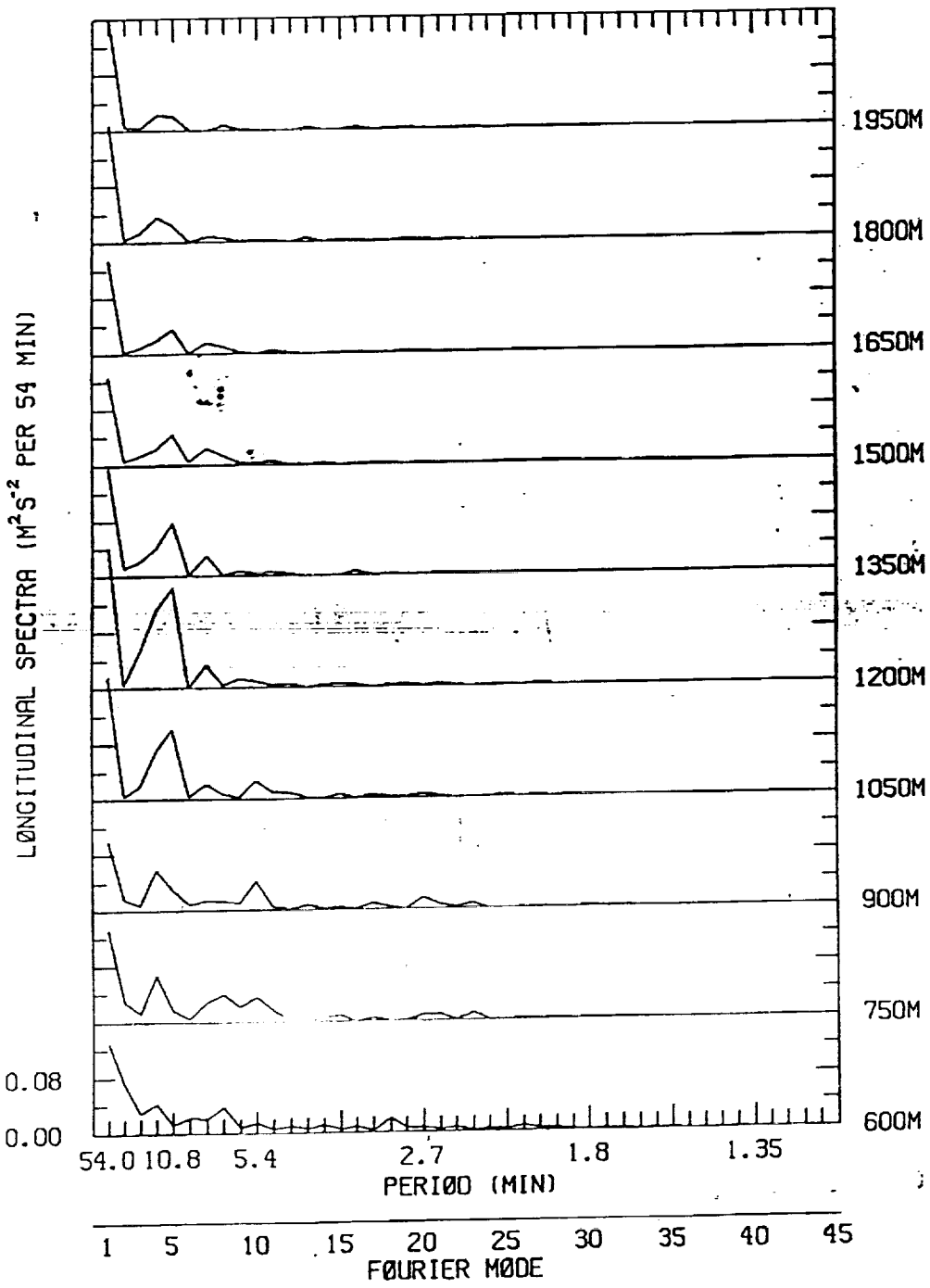
LØNGITUDINAL SPECTRA (M^2S^{-2} PER 54 MIN)
1950M
1800M
1650M
1500M
1350M
1200M
1050M
900M
750M
600M
0.08
0.00
54.0 10.8 5.4 2.7 1.8 1.35
PERIØD (MIN)
1 5 10 15 20 25 30 35 40 45
FØURIER MØDE

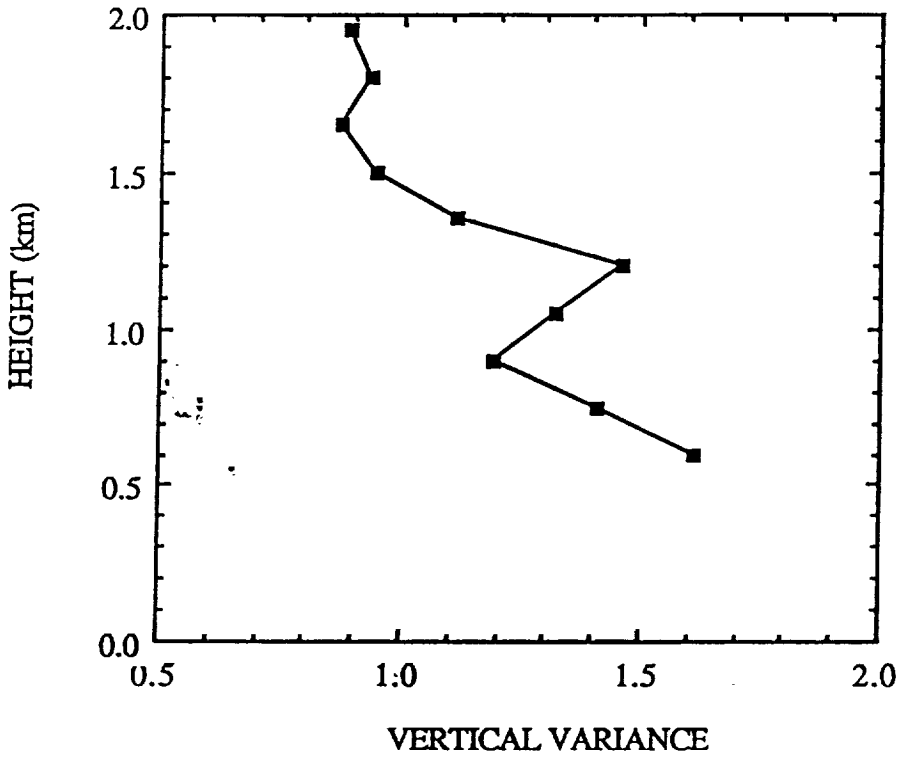
2.0
1.5
1.0
0.5
0.0
HEIGHT (km)
0.5
1.0
1.5
2.0
VERTICAL VARIANCE

12.

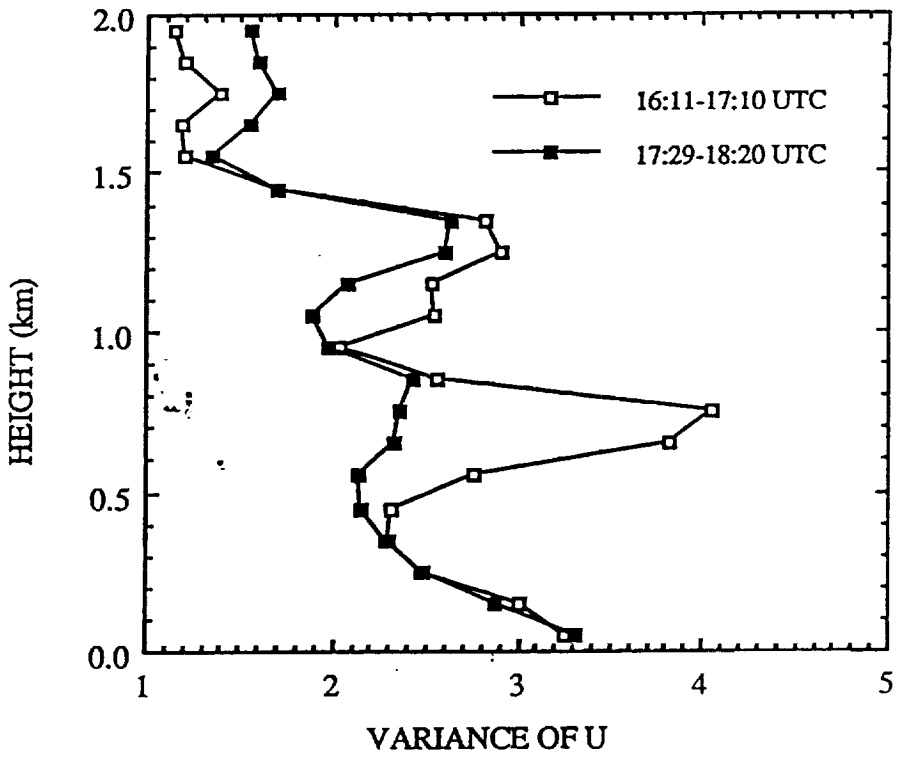
2.0
1.5
1.0
0.5
0.0
HEIGHT (km)
1
2
3
4
5
VARIANCE OF U
16:11-17:10 UTC
17:29-18:20 UTC

13

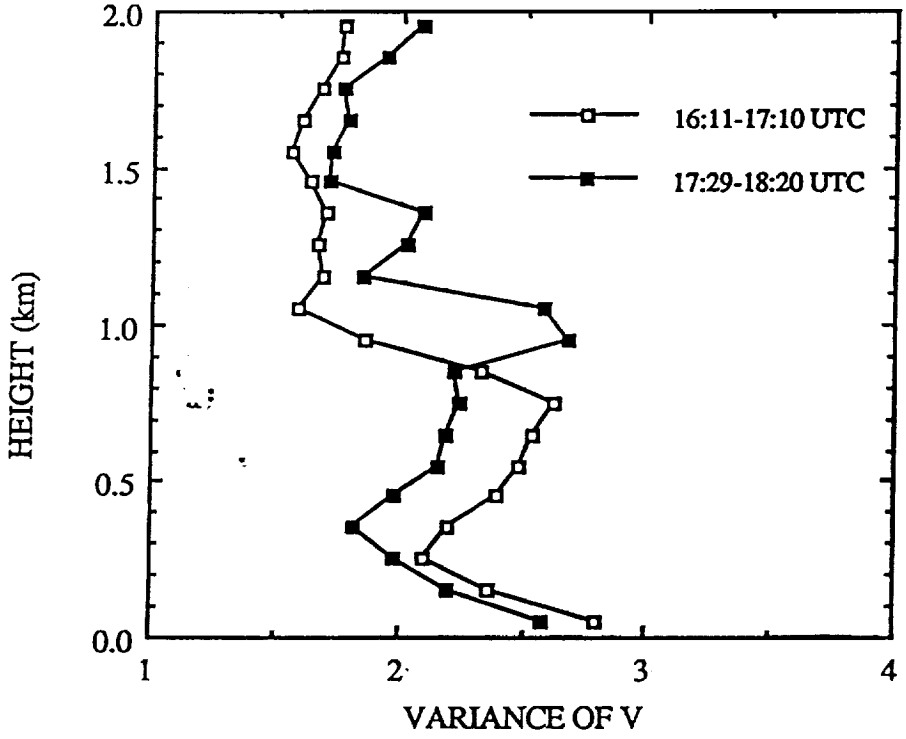
2.0
1.5
1.0
0.5
0.0
HEIGHT (km)
1
2
3
4
VARIANCE OF V
16:11-17:10 UTC
17:29-18:20 UTC

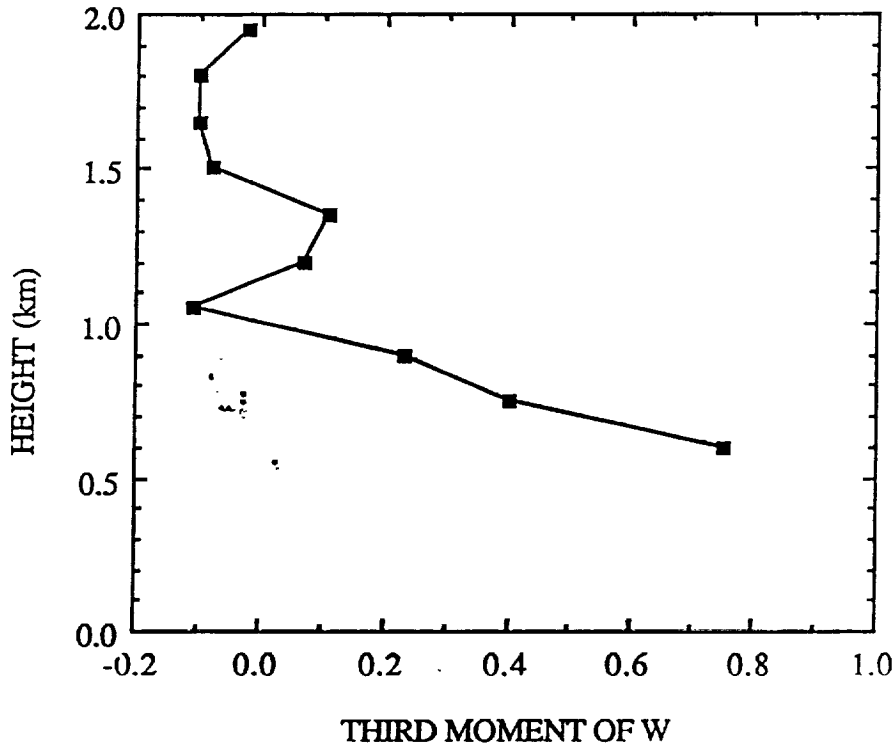
2.0
1.5
1.0
0.5
0.0
HEIGHT (km)
-0.2
0.0
0.2
0.4
0.6
0.8
1.0
THIRD MOMENT OF W

15

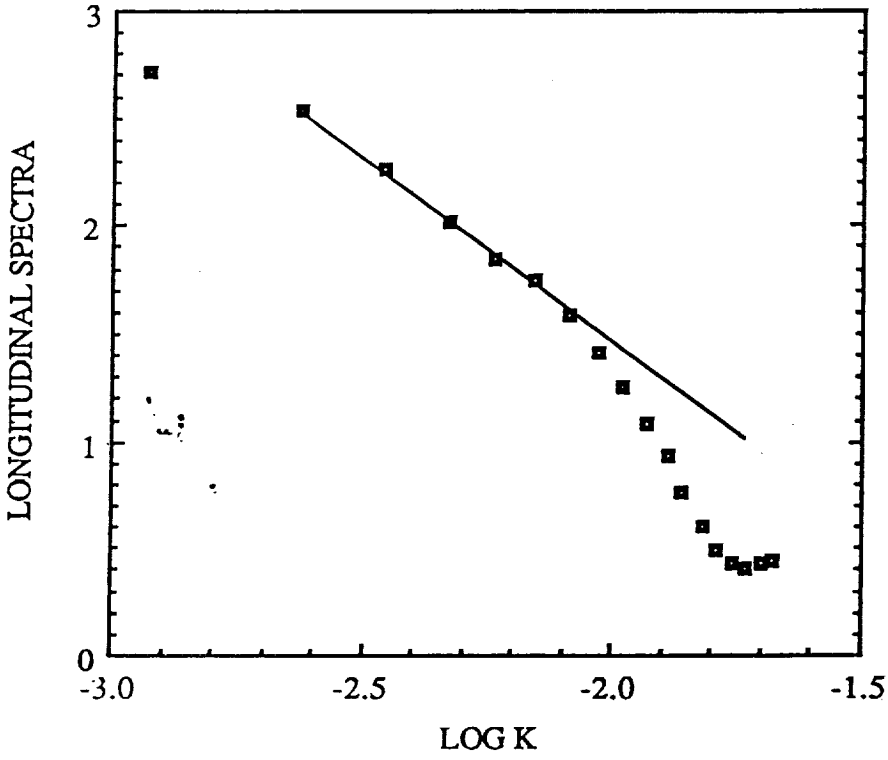

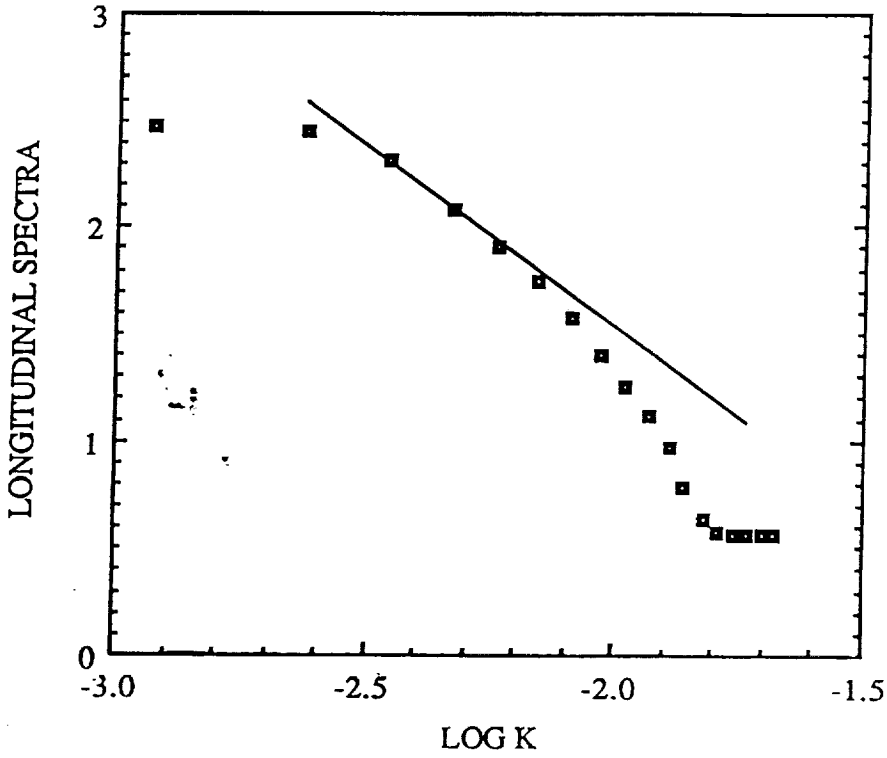
LONGITUDINAL SPECTRA
3
2
1
0
-3.0
-2.5
-2.0
-1.5
LOG K